Inorganic Chemistry

pubs.acs.org/IC

Article

Azo-Label Heterometal–Organic Rhomboids Exhibiting Photoswitchable NIR Luminescence in Crystalline State

Jing Xie,[‡] Ting Wu,[‡] Xiaoling Wang, Chengfeng Yu, Wei Huang, and Dayu Wu*

Cite This: https://dx.doi.org/10.1021/acs.inorgchem.0c02488

Read Online

ACCESS | Metrics & More | Article Recommendations | Supporting Information

ABSTRACT: Photochromism is an important strategy for realizing reversible light-controllable fluorescence switching. In spite of several reports on fluorescence switching via a photochromic process, the success of photochromic multimetallic complexes reversibly showing fluorescence switching in the solid or crystalline state has been limited for their application importance. Here, we report a photoswitchable near-infrared (NIR) fluorescence based on photochromism in the azo-label 3d/4f heterometal–organic rhomboids, **azo-Zn_2Ln_2** (Ln = Eu (**1**), Yb (**2**), and Er (**3**)), in the crystalline state. An individual metallorhomboid contains up to four azobenzene fragments, which is prepared via the three-component assembly of a *trans*-azobenzene-grafted multifunctional ligand, and 3d and 4f metal ions. The photoisomerization quantum yields of **azo-Zn_2Ln_2** complexes can be retained or even higher when compared to the free ligand due to the modification of electronic structure. The impressive crystalline-state NIR luminescence is observed for the complexes of azo-Zn_2Yb_2 (**2**) and azo-Zn_2Er_2 (**3**) at room temperature. Intriguingly, the switchable NIR luminescence can be effectively regulated by photochromism in the crystalline state. These features endow the self-assembly of the 3d/4f metallorhomboid with synergetic multifunctional behavior between photochromism and NIR luminescence.

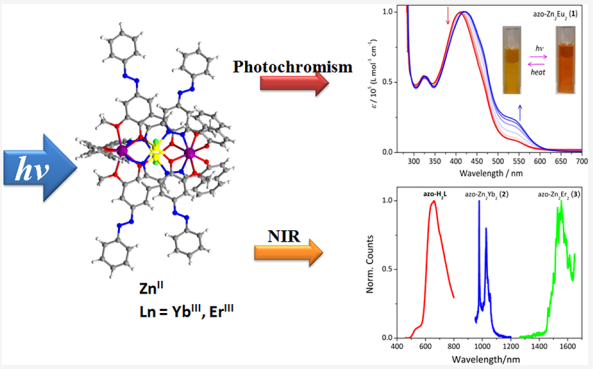

INTRODUCTION

Molecules with a bistable state such as azobenzene provide a prototypical molecular switch that can undergo reversible *trans*↔*cis* isomerization by external stimuli, such as light, heat, etc. Due to their photochromic properties, the pure organic azobenzene derivatives have many potential applications in fields, such as information storage,[1] molecular switches,[2] liquid crystal,[3] nonlinear optical,[4] and biological research.[5] Recently, the azobenzene-functionalized metal complexes have aroused wide attention, including azobenzen-functional ferrocene derivatives,[6,7] $Co^{III/II}$,[8] Fe^{II},[9] Zn^{II},[10] Ir^{III} complexes, etc.[11] By anchoring an azo moiety with a metal center, the multifunctional properties, including photochromism, redox, magnetism, etc., can be integrated.[12−16] The majority of complexes based on reversible photoisomerization belongs to the monometallic 3d-block transition-metal complexes. However, such metal complexes suffer from the reduced quantum yields of photoisomerization related to those of the organic azobenzenes, and the synergy effect between photochromism and other physical properties is still to be enhanced.

To improve the performance of azobenzene-functionalized metal complexes, we transfer our attention to metal–organic assembly by using 3d/4f hybrid metal ions instead of pure 3d-block transition-metal ions. In the presence of low extinction coefficients of the Laporte forbidden f–f transitions, lanthanide-based luminescence involves the efficient sensitization by virture of the suitable excited triplet state of the ligand. To our best knowledge, a limited number of azobenzene–lanthanide complexes have been reported to show lanthanide luminescence owing to the forbidden nature of their electronic transitions. Considering that lanthanide-based NIR emitters, such as Nd^{III}, Er^{III}, and Yb^{III}, are of particular interest for their potential applications in many fields, in the case of azobenzene–lanthanide complexes, we are interested in investigating the ability of functional azobenzene derivatives to regulate the sensitization of NIR-emitting lanthanides via photochromism.

In the previous work, we have reported the self-assembly of a 3d/4f metallorhomboid from a hydrazon-based asymmetric tribidendate ligand (H_2L).[17] It is reasoned that the presence of configuration twist enhanced the reversible thermal- and pressure-responsive luminescence from the organic chromophore. Unfortunately, the lanthanide-based luminescence in such 3d/4f complexes has not been observed at room

Received: August 20, 2020

temperature. The energy transfer cannot occur from the chromophore to the visible-emitting lanthanide centers, such as Eu^{3+} and Tb^{3+}; that is an obvious shortcoming in the fields of basic research and practical application. The emission optimization needs maximizing energy transfer from the sensitizing moiety to the lanthanoid by adjusting the energies of the lanthanide-center excited state. As a continuous work, here we report a photoswitchable 3d/4f metallorhomboid by integrating an azobenzene-label ligand (**azo-H_2L**, Scheme 1)

Scheme 1. Synthetic Procedure for the Preparation of Azo-H_2L

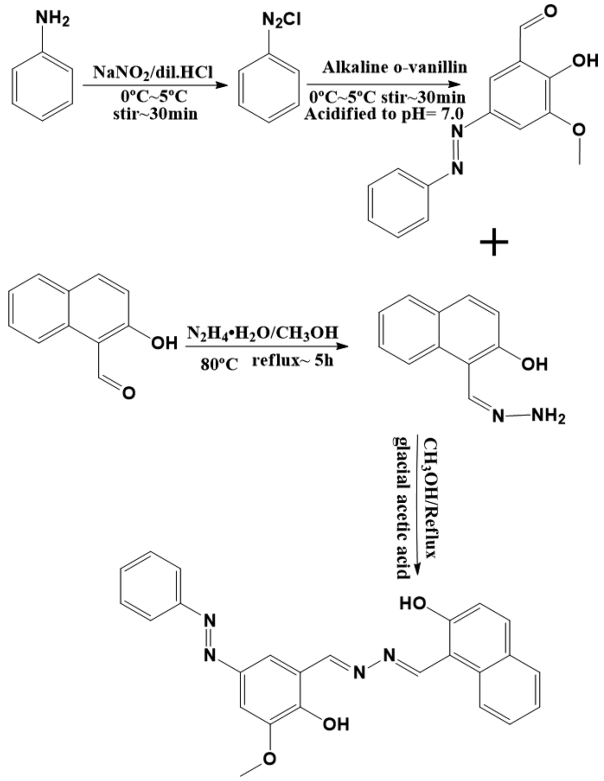

and the NIR-emitting lanthanoids (such as Yb^{3+}, Er^{3+}, etc.), owing to their lower excited energy compared to the visible-emitting lanthanoids. The modified ligand is grafted with an azo moiety, and the character of simultaneously chelating 3d and 4f metal ions is persistent to allow the formation of **azo-Zn_2Ln_2** metallorhomboid (Figure 1). This work represents a promising case of an azo-label multimetallic molecular crystal capable of generating a synergistic effect between efficient NIR photoluminescence and photochromism.

EXPERIMENTAL SECTION

Materials and General Procedures. All the reagents employed were commercially available and used without further purification. Methanol and dichloromethane were dried using standard procedures. 1-(Hydrazineylidenemethyl)-naphthalen-2-ol and 5-(2-phenyldiazenyl)-2-hydroxy-3-methoxybenzaldehyde were synthesized according to a literature method,[18,19] respectively.

Elemental analyses (C, H, and N) were conducted with a PerkinElmer 2400 analyzer. The IR spectra of polycrystalline solids were performed on a Nicolet Magna-IR 750 spectrophotometer in the 4000−400 cm^{-1} region (w, weak; b, broad; m, medium; s, strong) by KBr discs. UV−visible studies were performed in a PerkinElmer Lambda 950 UV−vis instrument. Powder X-ray diffraction (PXRD) was recorded on a RINT2000 vertical goniometer with a Cu Kα X-ray source (operated at 40 kV and 100 mA). Simulations of the powder diffractograms were calculated with CrystalDiffract (2015 CrystalMaker Software Ltd.) using the single crystal cif files. Fluorescence spectra were recorded on an Edinburgh FS5 instrument. The slit width was fixed at 1 nm for both excitation and emission light. Emission and excitation spectra were corrected for the spectral response of the monochromator and the detector, using typical correction spectra provided by the manufacturer.

Crystal Structure Determination. The diffraction intensity data of azo-Zn_2Eu_2 (**1**) and azo-Zn_2Er_2 (**3**) at 173 K were collected on a Bruker APEX-2 CCD with graphite-monochromated Mo Kα radiation (λ = 0.71073 Å). Data collection, data reduction, and cell refinement were performed by using the Bruker Instrument Service v4.2.2 and SAINT V8.34A software.[20,21] Structure was solved using direct methods with the SHELXS program. Refinement was performed using SHELXL based on F^2 through the full-matrix least-squares routine.[22] Absorption corrections were applied using the multiscan program SADABS.[23] Hydrogen atoms of organic ligands were generated geometrically by the riding mode, and all the non-hydrogen atoms were refined anisotropically through full-matrix least-squares technique on F^2 with the SHELXTL program package.[24,25] A summary of the crystallographic data and refinement parameters is given in Table 1.

Calculation of Photoisomerization Quantum Yields and Isomerization Rate Constants. The commercial UV light with wavelength at 254 and 365 nm was used in the experiment. A 1 cm path length quartz cell was used for the photoisomerization measurements. The sample concentration was approximately 2.0 × 10^{-5} M for all complexes.

We introduced the first-order kinetic eq 1 to study the photoisomerization dynamics as follows[26]

$$\ln \frac{A_\infty - A_0}{A_\infty - A_t} = k_{iso}t \tag{1}$$

wherein A_∞, A_0, and A_t represent the saturated absorbance, the absorbance before and after illumination, respectively. By plotting the value on the left side of the above equation with respect to time (t), a linear function was obtained. From the data, the isomerization reaction conforms to the first-order reaction dynamics equation and the slope was its rate constant k_{iso}. The data rate constants (k_{iso}) for all complexes were the average of the three independent replicates performed for each concentration.

The photoisomerization quantum yield was evaluated based on the following eq 2[27]

$$\Phi = k_0 \frac{1}{I_0} \frac{1}{1 - 10^{-\varepsilon c l}} \tag{2}$$

where k_0 is a zero-order rate constant for the initial isomer concentration in mol L^{-1} s^{-1}, I_0 is the intensity of incident irradiation light in einstein L^{-1} s^{-1}, ε is the extinction coefficient in L mol^{-1} cm^{-1} at the irradiation wavelength of the solution, c is the concentration of solution in mol L^{-1}, and l is the path length of light through the sample in cm. The k_0 is given by eq 3

$$A_0 - A_t = k_0 t \tag{3}$$

Synthesis of Ligand azo-H_2L. The mixture of 1-(hydrazineylidenemethyl)-naphthalen-2-ol (0.43 g, 2.31 mmol) and 5-(2-phenyldiazenyl)-2-hydroxy-3-methoxybenzaldehyde (0.58 g, 2.26 mmol) in 60 mL of ethanol was heated at 80 °C in the presence of 0.5 mL of glacial acetic acid for 6 h. The orange solid was filtered and recrystallized from ethanol to obtain **azo-H_2L**. Yield: ca. 85%. Elemental analysis (%) calculated for $C_{25}H_{20}N_4O_3$: C, 70.74; H, 4.75; N, 13.20; Found: C, 71.02; H, 4.73; N, 13.14; IR (KBr, cm^{-1}): 3520(w), 1609(s), 1549(w), 1462(s), 1395(w), 1318(s), 1270(s), 1189(m), 1149(w), 1122(s), 1086(w), 974(m), 868(m), 808(s), 768(m), 743(s), 686(s), 429(m). ^{1}H NMR (400 MHz, $CDCl_3$) δ 12.94 (s, 1H), 12.24 (s, 1H), 9.68 (s, 1H), 8.92 (s, 1H), 8.18 (d, J = 8.6 Hz, 1H), 7.95 (dd, J = 8.3, 3.9 Hz, 3H), 7.85 (d, J = 8.0 Hz, 1H),

https://dx.doi.org/10.1021/acs.inorgchem.0c02488
Inorg. Chem. XXXX, XXX, XXX−XXX

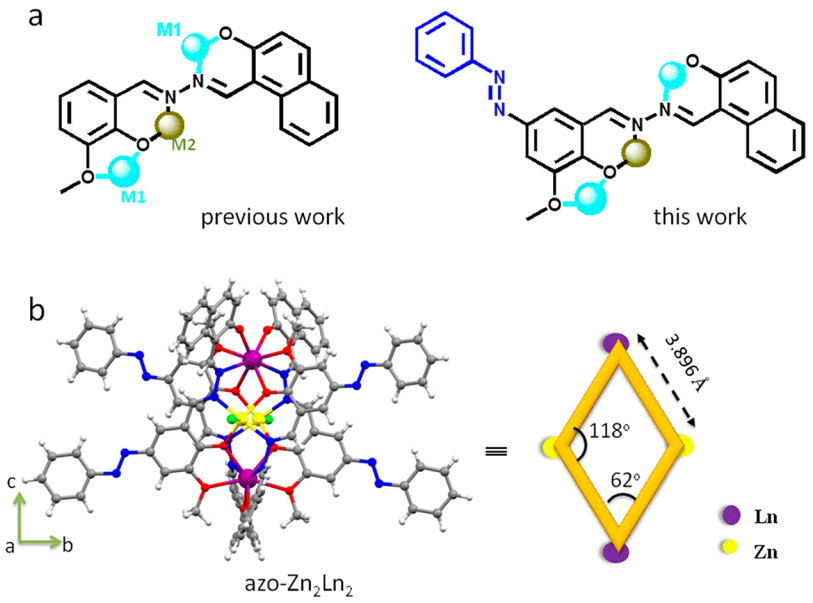

Figure 1. (a) The metal binding mode of $\mathbf{Zn_2Ln_2}$ in the previous work[17] and in the photoswitchable metal−organic rhomboid. (b) Sphere and stick representation of the crystal structure of azo-Zn_2Eu_2 (**1**) at 173 K with the 30% thermal ellipsoids showing the *trans*-azo configuration (all hydrogen atoms are omitted for clarity; color system: Eu (purple), Zn (yellow), N (blue), Cl (green), C (gray)) as well as the simplified **azo-Zn_2Ln_2** (**1**) rhomboid, in which Ln···Zn separation of 3.896 Å and inner angle of 118° and 62°, respectively.

Table 1. Crystallographic Data and Structure Refinement for Azo-Zn_2Eu_2 (1) and Azo-Zn_2Er_2 (3)

parameter	value/remark	
empirical formula	$C_{100}H_{72}Cl_2N_{16}O_{26}Zn_2Eu_2$	$C_{100}H_{72}Cl_2N_{16}O_{27}Zn_2Er_2$
formula weight	2419.29	2465.89
temperature (K)	173	
wavelength (Å)	0.71073	
space group	orthorhombic	
space group	F_{ddd}	
a (Å)	15.6755(6)	15.7257(5)
b (Å)	26.5672(6)	26.2958(7)
c (Å)	54.2951(12)	54.2689(17)
V (Å^3)	22611.4(11)	22441.3(12)
Z	8	
F (000)	9696	9840
ρ_{calcd} [g cm^{-3}]	1.421	1.460
μ (Mo Kα) [mm^{-1}]	1.636	2.027
goodness-of-fit[a] on F^2	1.042	1.028
R_1, wR_1 ($I > 2\sigma(I)$[b]	0.0329, 0.1056	0.0524, 0.1559
R_2, wR_2 (all data)	0.0398, 0.1091	0.0786, 0.1794

[a]GOF = $[\sum[w(F_o^2 - F_c^2)^2]/(N_{obs} - N_{params})]^{1/2}$, based on the data $I > 2\sigma(I)$. [b]$R_1 = \sum||F_o| - |F_c||/\sum|F_o|$; $wR_2 = [\sum[w(F_o^2 - F_c^2)^2]/\sum[w(F_0^2)^2]]^{1/2}$.

7.78 (d, J = 2.0 Hz, 1H), 7.71 (d, J = 1.8 Hz, 1H), 7.65 (t, J = 7.9 Hz, 1H), 7.50 (ddd, J = 19.0, 16.2, 7.6 Hz, 5H), 4.10 (s, 3H).

Synthesis of azo-[Zn_2Ln_2]. All three complexes were synthesized by the similar method as follows: A mixture of **azo-H_2L** (0.1 mmol, 0.0424 g), $LnCl_3{\cdot}6H_2O$ (0.1 mmol) in 15 mL of CH_3OH in the presence of triethylamine (0.4 mmol, 56 μL) was stirred for several minutes, and Zn $(OAc)_2{\cdot}2H_2O$ (0.1 mmol, 0.0220 g) was then added. The precipitation will become clear upon addition of 15 mL of CH_2Cl_2. The resulting clear yellow solution was stirred briefly and filtered; the orange block crystals suitable for X-ray diffraction studies were obtained by slow diffusion of ether into a solution of the complexes in CH_2Cl_2 after 1 week.

*azo-[Zn_2Eu_2] (**1**).* Yield: ca. 68%. Elemental analysis (%) calculated for $C_{100}H_{72}Cl_2N_{16}O_{12}Zn_2Eu_2$: C, 54.71; H, 3.31; N, 10.21; Found: C, 54.54; H, 3.28; N, 10.24; IR (KBr, cm^{-1}): 3446(w), 1606(s), 1571(m), 1534(s), 1455(s), 1425(m), 1388(m), 1358(m), 1343(w), 1310(w), 1281(w), 1248(s), 1189(m), 1124(m), 947(m), 830(m), 815(m), 743(m), 683(m), 664(w), 506(m), 474(m), 424(m).

*azo-[Zn_2Yb_2] (**2**).* Yield: ca. 56%. Elemental analysis (%) calculated for $C_{100}H_{72}Cl_2N_{16}O_{12}Zn_2Yb_2$: C, 53.68; H, 3.24; N, 10.02; Found: C, 53.56; H, 3.35; N, 10.12; IR (KBr, cm^{-1}): 3430(w), 1615(s), 1573(m), 1534(s), 1462(s), 1428(w), 1384(m), 1365(m), 1312(w), 1254(s), 1192(m), 1129(m), 1025(m), 951(w), 831(m), 762(m), 688(m), 667(w), 512(m), 478(m), 429(m).

*azo-[Zn_2Er_2] (**3**).* Yield: ca. 65%. Elemental analysis (%) calculated for $C_{100}H_{72}Cl_2N_{16}O_{12}Zn_2Er_2$: C, 53.96; H, 3.26; N, 10.07; Found: C, 53.82; H, 3.33; N, 10.12; IR (KBr, cm^{-1}): 3425(w), 1615(s), 1573(m), 1539(s), 1451(s), 1425(m), 1391(m), 1361(m), 1310(w), 1284(w), 1250(w), 1187(m), 1127(m), 1095(m), 947(s), 834(m), 743(m), 686(m), 639(w), 619(w), 572(w), 475(m), 428(m).

https://dx.doi.org/10.1021/acs.inorgchem.0c02488
Inorg. Chem. XXXX, XXX, XXX−XXX

RESULTS AND DISCUSSION

Suitable crystals of the complexes azo-Zn_2Eu_2 (**1**) and azo-Zn_2Er_2 (**3**) are obtained by slow diffusion of ether into a solution of the complexes in CH_2Cl_2. Single-crystal X-ray diffraction (XRD) analysis of complexes **1** and **3** showed that they are isostructural. The purity of bulk samples of **1**−**3** was confirmed through powder XRD patterns (SI Figure S1). As representative, the crystal structure of complex **1** at 173 K is presented in Figure 1b. Complex azo-Zn_2Eu_2 (**1**) crystallized in the orthorhombic *Fddd* space group and showed a tetranuclear rhomboid structure with an ideal D_2 symmetry. The asymmetric unit contains half Eu^{3+}, half Zn^{2+}, and one full ligand. Four azo-grafted ligands are found to lose all the protons on hydroxyl groups and form the dianion **azo-L**$^{2-}$ in the resulting complexes. In the rhomboid, the edge of Zn···Eu is 3.896(2) Å and the inner angle is 117.57° and 62.43°, respctively, indicating the nearly perfect rhomboid structure. The Ln atom maintains the coordination environment by six O atoms (O1, O2, O3) and two N1 atoms, favoring a shielding from solvent molecules. As expected, the azobenzene block presents in the form of *trans*-conformation. The length of the N═N bond in complex **1** is 1.257 Å, which is consistent with the corresponding distance observed for azobenzene and its derivatives.[28]

The UV−vis absorption spectra of free ligand **azo-H_2L** and its complex azo-Zn_2Eu_2 (**1**) in DMF at room temperature are depicted in Figure 2. The analysis of the spectra of azo-free and

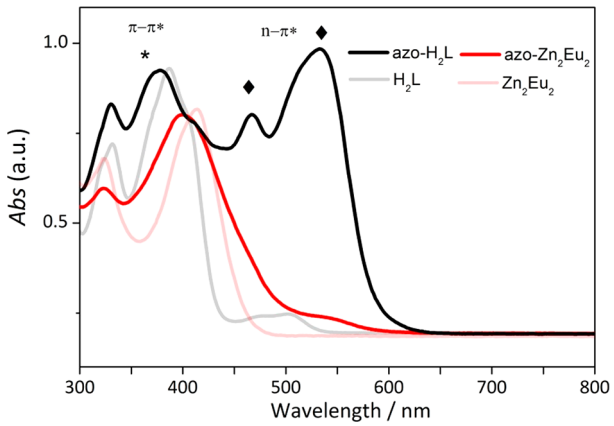

Figure 2. Electronic absorption spectra of **azo-H_2L** and its complex azo-Zn_2Eu_2 (**1**) as well as their azo-free counterparts in DMF (2.0×10^{-5} M).

azo-label ligands indicates the additional peaks at 376 nm and at 532 and 467 nm in **azo-H_2L** are tentatively ascribed to $\pi-\pi^*$ and $n-\pi^*$ transition bands of the azo group, respectively. The absorption bands of the complexes, includingZn_2Eu_2 and azo-Zn_2Eu_2 (**1**), are significantly different from those of the free ligands. The UV−vis absorption spectrum of the complex azo-Zn_2Eu_2 (**1**) exhibits a strong merged peak at 400 nm and a weak peak at 550 nm, which involve the superposition of $\pi-\pi^*$ and $n-\pi^*$ transitions. Absorption spectra are also checked in other solvents, such as DMSO, CH_3OH, and acetonitrile, and in solid (SI Figures S2 and S3). In the solid state, the absorption spectra of the azo ligand and its metal complex become broad with low resolution compared to those in solutions. This should be induced by the strong $\pi\cdots\pi$ stacking interactions of neighboring azo moieties, as indicated in the analysis of X-ray diffraction structures (SI Figures S4 and S5).

Figure 3 shows the apparent spectral change of **azo-H_2L** and its complex azo-Zn_2Eu_2 (**1**) in DMF solution, which are

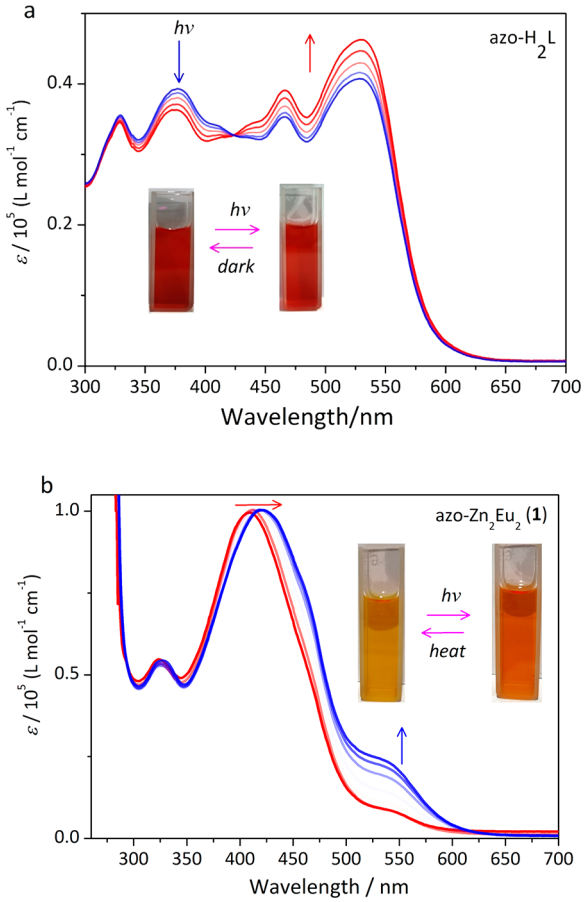

Figure 3. Reversible UV/vis spectral changes induced by light and heat or darkness in solution. (a) Spectral change of **azo-H_2L** upon irradiation at 365 nm within 2 h. (b) Spectral change of complex azo-Zn_2Eu_2 (**1**) upon irradiation at 254 nm. The insets show the reversible color changes of the azo ligand and heterometal−organic rhomboid to light and darkness or heat.

subject to UV irradiation as a function of time. As shown in Figure 3a, upon a 365 nm UV-light irradiation, the absorbance of the $\pi-\pi^*$ band at 376 nm significantly decreases with an concomitant increase of $n-\pi^*$ band at 467 and 532 nm, which are typical *trans*-to-*cis* isomerization of the azobenzene moiety. Subsequently, the spectral is reversed in the dark, indicating a *cis*-to-*trans* isomerization.

Relative to that of the azo ligand, the $\pi-\pi^*$ transition in metal complex azo-Zn_2Eu_2 (**1**) shifts to lower energy of ca. 20 nm due to the metal-coordination induced twist as well as the deprotonation of the ligand. Therefore, the energy levels between the $\pi-\pi^*$ and the $n-\pi^*$ overlap, resulting in the competitive spectral response to light or heat as far as the absorption intensity is concerned. Intriguingly, the absorption band with a peak at ca. 400 nm exhibits an obvious red shift of ca. 20 nm upon UV irradiation. Simultaneously, the band with a peak at 500 nm continues to obtain its intensity (Figure 3b). Hence, the more substantial color change of the metal complex is observed than that of the free ligand (**azo-H_2L**) due to *trans*-to-*cis* isomerization (inset of Figure 3), which favors the naked-

https://dx.doi.org/10.1021/acs.inorgchem.0c02488
Inorg. Chem. XXXX, XXX, XXX−XXX

eye detection of the photochromic properties of azo-label metallorhomboids. The photochromic property of **1** is further investigated in the crystalline state because the solid-state performance is crucial to practical applications (SI Figure S6). The electronic absorption spectra of the sample that is subjected to UV irradiation shows the similar result with those of solution. The results indicate the photochromism in crystalline solid is also effective despite the relatively low efficiency compared to that in solution.

In order to investigate the photoisomerization dynamics (for details, see the Experimental Section), the rate constants of the photoisomerization reaction for **azo-H_2L** and azo-Zn_2Eu_2 (**1**) are calculated to be 2.0×10^{-4} and 1.5×10^{-4} s^{-1} by employing the first-order kinetic equation (SI Figure S7), which fall within the normal range for azobenzene and its derivatives (10^{-4}–10^{-5} s^{-1}).[29,30] The photoreaction quantum yields ($\Phi_{t\rightarrow c}$) is also evaluated for **azo-H_2L** and azo-Zn_2Eu_2 (**1**) to be 0.0125 and 0.0335, respectvely. Hence, the *trans*-to-*cis* photoisomerization quantum yields of the metallorhomboid is even higher than that of its pure ligand. Compared with other azobenzene-containing metal complexes, such type of 3d/4f metal complexes exhibit more sensitive photoisomerization.[31]

The photoluminescence properties of the azo ligand and its complexes were investigated before and after UV-light irradiation at room temperature. The ligand **azo-H_2L** emits the similar red luminescence with a peak at ca. 650 nm in both solution and solid state (Figure 4 and SI Figure S8). The decrease of ca. 50% in its PL intensity occurs upon UV-light irradiation. The luminescence can be recovered after heating the sample at 120 °C for several minutes, indicating a reversible response to light. It could be noticed that the energy levels are likely not suitable for sensitization of the visible emitting lanthanides, but should be high enough to sensitize the near-infrared emitters, such as Yb(III), Er(III), etc.[32,33] Therefore, the analogue complexes, azo-Zn_2Yb_2 (**2**) and azo-Zn_2Er_2 (**3**), were prepared in the similar manner to that of azo-Zn_2Eu_2 (**1**) and their NIR photoluminescences were studied. As expected, the Eu(III) complex **1** is nonemissive either in solution or in the solid state. It should be noted that the solvent had a very strong influence on the intensity of NIR spectra. The PL intensity of complexes **2** and **3** is very weak or even negligible in organic solutions, such as CH_3CN and DMF, which is likely due to quenching by the C–H oscillators of the solvents.[34] Hence, we directly investigate the crystalline-state PL spectra before and after UV-light irradiation considering the photochromism simultaneously occurs in the solid state. As shown in Figure 5, the complex **2** exhibits the characteristic band of Yb(III) with a main sharp peak at 980 nm and a wide shoulder centered at 1026 nm, which should be attributed to the $^2F_{5/2} \rightarrow {}^2F_{7/2}$ transition for the Yb(III) center.[35] The splitting of the energy levels of the Yb(III) ion in metal complexes has been frequently evidenced as a consequence of the ligand field effect.[36,37] In complex azo-Zn_2Er_2 (**3**), a characteristic peak at 1530 nm is observed, which is attributed to the $^4I_{13/2} \rightarrow {}^4I_{15/2}$ transition.[38] The corresponding excitation spectra of Yb(III) and Er(III) complexes are in total agreement with the absorption spectra, demonstrating that an antenna effect is responsible for the sensitized NIR emission due to energy transfer from the ligand to the Ln cations. Hence, the complexes azo-Zn_2Yb_2 (**2**) and azo-Zn_2Er_2 (**3**) exhibit strong NIR emission in the crystalline state.[39,40] More attractively, the NIR luminescence intensity continues to decrease, subjected to irradiation with UV-light, which is indicative of the sensitive response of NIR emission via photoisomerization even in the crystalline state. Upon annealing the sample, the NIR emissive intensity almost recovers to the initial state, suggesting the reversibility of the photoswitchable NIR luminescence.

In conclusion, the multicomponent self-assembly can be extended to the photofunctional systems. In this work, we show how we can systematically modify synergetic properties, including photochromism and NIR luminescence in the sophiscated metal complexes. The inertness of the tribidendate

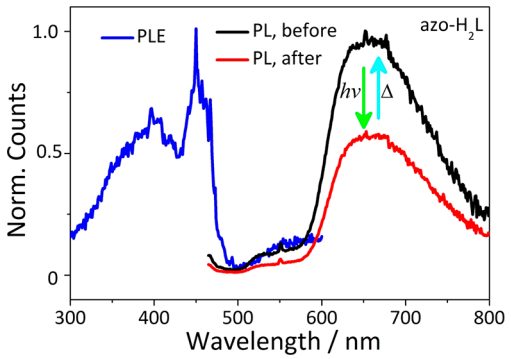

Figure 4. Excitation (PLE) and emission spectra (PL) of ligand, **azo-H_2L**, with λ_{ex} = 450 nm before and after UV-light irradiation at 365 nm in solution (10^{-5} mol/L).

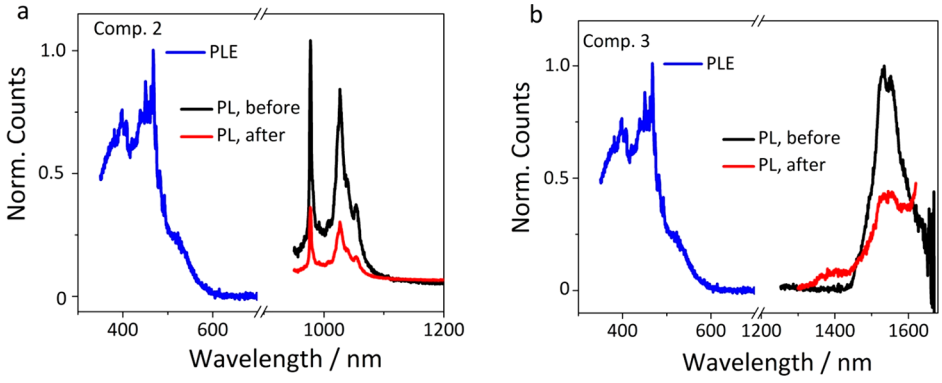

Figure 5. Excitation (PLE) and emission spectra (PL) of azo-Zn_2Yb_2 (**2**) and azo-Zn_2Er_2 (**3**) in the crystalline state with λ_{ex} = 468 nm before and after UV-light irradiation for 10 min at room temperature.

https://dx.doi.org/10.1021/acs.inorgchem.0c02488
Inorg. Chem. XXXX, XXX, XXX–XXX

donor maintains the nearly perfect metallorhomboid structure and provides the possibility of changing both the functional groups and the lanthanide ion for the sensitization of the NIR-emitting lanthanide center (Ln = Yb(III), Er(III)). This strategy produces a family of multimetallic molecules with synergistic photoresponsive properties by labeling the azo moiety in the 3d/4f metallorhomboid. Our current results represent a new way of photochromism-modulated NIR luminescence utilizing the multimetallic molecular platforms.

■ ASSOCIATED CONTENT

Supporting Information

The Supporting Information is available free of charge at https://pubs.acs.org/doi/10.1021/acs.inorgchem.0c02488.

Additional UV−vis spectra, PL spectra, and powder XRD spectra (PDF)

Accession Codes

CCDC 1977811 and1977812 contain the supplementary crystallographic data for this paper. These data can be obtained free of charge via www.ccdc.cam.ac.uk/data_request/cif, or by emailing data_request@ccdc.cam.ac.uk, or by contacting The Cambridge Crystallographic Data Centre, 12 Union Road, Cambridge CB2 1EZ, UK; fax: +44 1223 336033.

■ AUTHOR INFORMATION

Corresponding Author

Dayu Wu − *Jiangsu Key Laboratory of Advanced Catalytic Materials and Technology, Advanced Catalysis & Green Manufacturing Collaborative Innovation Center, School of Petrochemical Engineering, Changzhou University, Changzhou, Jiangsu 213164, P. R. China;* orcid.org/0000-0002-4132-4795; Email: wudy@cczu.edu.cn

Authors

Jing Xie − *Jiangsu Key Laboratory of Advanced Catalytic Materials and Technology, Advanced Catalysis & Green Manufacturing Collaborative Innovation Center, School of Petrochemical Engineering, Changzhou University, Changzhou, Jiangsu 213164, P. R. China*

Ting Wu − *Jiangsu Key Laboratory of Advanced Catalytic Materials and Technology, Advanced Catalysis & Green Manufacturing Collaborative Innovation Center, School of Petrochemical Engineering, Changzhou University, Changzhou, Jiangsu 213164, P. R. China*

Xiaoling Wang − *Jiangsu Key Laboratory of Advanced Catalytic Materials and Technology, Advanced Catalysis & Green Manufacturing Collaborative Innovation Center, School of Petrochemical Engineering, Changzhou University, Changzhou, Jiangsu 213164, P. R. China*

Chengfeng Yu − *Jiangsu Key Laboratory of Advanced Catalytic Materials and Technology, Advanced Catalysis & Green Manufacturing Collaborative Innovation Center, School of Petrochemical Engineering, Changzhou University, Changzhou, Jiangsu 213164, P. R. China*

Wei Huang − *Jiangsu Key Laboratory of Advanced Catalytic Materials and Technology, Advanced Catalysis & Green Manufacturing Collaborative Innovation Center, School of Petrochemical Engineering, Changzhou University, Changzhou, Jiangsu 213164, P. R. China*

Complete contact information is available at: https://pubs.acs.org/10.1021/acs.inorgchem.0c02488

Author Contributions

‡These authors contributed equally to this work.

Notes

The authors declare no competing financial interest.

■ ACKNOWLEDGMENTS

We are thankful for financial support by the PAPD of Jiangsu Higher Education Institutions. This work was supported by the NSFC program (Grant 21671027).

■ REFERENCES

(1) Wang, D.; Ye, G.; Wang, X.; Wang, X. Graphene functionalized with azo polymer brushes: Surface-initiated polymerization and photoresponsive properties. *Adv. Mater.* **2011**, *23*, 1122−1125.

(2) Nacci, C.; Baroncini, M.; Credi, A.; Grill, L. Reversible photoswitching and isomer-dependent diffusion of single azobenzene tetramers on a metal surface. *Angew. Chem., Int. Ed.* **2018**, *57*, 15034−15039.

(3) Wani, O. M.; Verpaalen, R.; Zeng, H.; Priimagi, A.; Schenning, A. P. H. J. An artificial nocturnal flower *via* humidity-gated photoactuation in liquid crystal networks. *Adv. Mater.* **2019**, *31*, 1805985.

(4) Miniewicz, A.; Girones, J.; Karpinski, P.; Mossety-Leszczak, B.; Galina, H.; Dutkiewicz, M. Photochromic and nonlinear optical properties of azo-functionalized POSS nanoparticles dispersed in nematic liquid crystals. *J. Mater. Chem. C* **2014**, *2*, 432−440.

(5) Zhang, F.; Zarrine-Afsar, A.; Al-Abdul-Wahid, M. S.; Prosser, R. S.; Davidson, A. R.; Woolley, G. A. Structure-based approach to the photocontrol of protein folding. *J. Am. Chem. Soc.* **2009**, *131*, 2283−2289.

(6) Zhang, R.; Ji, Y. J.; Yang, L.; Zhang, Y.; Kuang, G. C. A ferrocene-azobenzene derivative showing unprecedented phase transition and better solubility upon UV irradiation. *Phys. Chem. Chem. Phys.* **2016**, *18*, 9914−9917.

(7) Yan, J. F.; Lin, D. Q.; Wang, X. G.; Wu, K. Q.; Xie, L. L.; Yuan, Y. F. Ferrocenylethynyl-terminated azobenzenes: Synthesis, electrochemical, and photoisomerization studies. *Chem. - Asian J.* **2015**, *10*, 614−621.

(8) Kume, S.; Kurihara, M.; Nishihara, H. Reversible trans-cis photoisomerization of azobenzene-attached bipyridine ligands coordinated to cobalt using a single UV light source and the Co(III)/Co(II) redox change. *Chem. Commun.* **2001**, 1656−1657.

(9) Yamamura, M.; Yamakawa, K.; Okazaki, Y.; Nabeshima, T. Coordination-driven macrocyclization for locking of photo- and thermal cis-trans isomerization of azobenzene. *Chem. - Eur. J.* **2014**, *20*, 16258−16265.

(10) Guezguez, I.; Ayadi, A.; Ordon, K.; Iliopoulos, K.; Branzea, D. G.; Migalska-Zalas, A.; Makowska-Janusik, M.; El-Ghayoury, A.; Sahraoui, B. Zinc induced a dramatic enhancement of the nonlinear optical properties of an azo-based iminopyridine ligand. *J. Phys. Chem. C* **2014**, *118*, 7545−7553.

(11) Perez-Miqueo, J.; Telleria, A.; Munoz-Olasagasti, M.; Altube, A.; Garcia-Lecina, E.; de Cozar, A.; Freixa, Z. Azobenzene-functionalized iridium(III) triscyclometalated complexes. *Dalton Trans.* **2015**, *44*, 2075−2091.

(12) Liu, H.; Xie, Z.-X.; Lu, J.; Han, Y.-F.; Wei, Y.-Q.; Guo, G.-C. A dual-emitting inorganic-organic hybrid material with emission intensity enchanced via electron-transfer photochromism. *Dyes Pigm.* **2020**, *181*, 108441−108446.

(13) Bisoyi, H. K.; Li, Q. Light-driven liquid crystalline materials: from photo-induced phase transitions and property modulations to applications. *Chem. Rev.* **2016**, *116*, 15089−15166.

(14) Cai, L.-Z.; Chen, Q.-S.; Zhang, C.-J.; Li, P.-X.; Wang, M.-S.; Guo, G.-C. Photochromism and photomagnetism of a 3d−4f hexacyanoferrate at room temperature. *J. Am. Chem. Soc.* **2015**, *137*, 10882−10885.

(15) Li, P.-X.; Wang, M.-S.; Zhang, M.-J.; Lin, C.-S.; Cai, L.-Z.; Guo, S.-P.; Guo, G.-C. Electron-transfer photochromism to switch bulk

second-order nonlinear optical properties with high contrast. *Angew. Chem., Int. Ed.* **2014**, *53*, 11529−11531.
(16) Sun, C.; Xu, G.; Jiang, X.-M.; Wang, G.-E.; Guo, P.-Y.; Wang, M.-S.; Guo, G.-C. Design strategy for improving optical and electrical properties and stability of lead-halide semiconductors. *J. Am. Chem. Soc.* **2018**, *140*, 2805−2811.
(17) Nie, Q.; Xie, Y.; Huang, W.; Wu, D. A Dynamic heterometal-organic rhomboid exhibiting thermochromic and piezochromic luminescence. *Inorg. Chem.* **2018**, *57*, 14489−14492.
(18) Chen, C. Y.; Lin, T. P.; Chen, C. K.; Lin, S. C.; Tseng, M. C.; Wen, Y. S.; Sun, S. S. New Chromogenic and Fluorescent Probes for Anion Detection: Formation of a [2 + 2] supramolecular complex on addition of fluoride with positive homotropic cooperativity. *J. Org. Chem.* **2008**, *73*, 900−911.
(19) Banerjee, S.; Brandao, P.; Saha, A. A robust fluorescent chemosensor for aluminium ion detection based on a Schiff base ligand with an azo arm and application in a molecular logic gate. *RSC Adv.* **2016**, *6*, 101924−101936.
(20) *SAINT*, v8.34A; Bruker AXS Inc.: Madison, WI, 2013.
(21) *APEX2*, v2014.5-0; Bruker AXS Inc.: Madison, WI, 2007.
(22) *SADABS*; Bruker AXS Inc.: Madison, WI, 2014.
(23) Sheldrick, G. M. A short history of SHELX. *Acta Crystallogr., Sect. A: Found. Crystallogr.* **2008**, *64*, 112−122.
(24) *SHELXTL VS.1, Software Reference Manual*; Bruker, AXS, Inc.: Madison, WI. 1997.
(25) Spek, A. L. J. Single-crystal structure validation with the program PLATON. *J. Appl. Crystallogr.* **2003**, *36*, 7−13.
(26) Suh, E. H.; Liu, Y.; Connelly, S.; Genereux, J. C.; Wilson, I. A.; Kelly, J. W. Stilbene vinyl sulfonamidesas fluorogenic sensors of and traceless covalent kinetic stabilizers of transthyretin that preventamyloidogenesis. *J. Am. Chem. Soc.* **2013**, *135*, 17869−17880.
(27) Sierocki, P.; Maas, H.; Dragut, P.; et al. Photoisomerization of azobenzene derivatives innanostructured silica. *J. Phys. Chem. B* **2006**, *110*, 24390−24398.
(28) Gajda, K.; Zarychta, B.; Daszkiewicz, Z.; Domanski, A. A.; Ejsmont, K. Substituent effects in *trans*-p, p′-disubstituted azobenzenes: X-ray structures at 100 K and DFT-calculated structures. *Acta Crystallogr., Sect. C: Struct. Chem.* **2014**, *C70*, 575−579.
(29) Yutaka, T.; Mori, I.; Kurihara, M.; Mizutani, J.; Kubo, K.; Furusho, S.; Matsumura, K.; Tamai, N.; Nishihara, H. Synthesis, characterization, and photochemical properties of azobenzene-conjugated Ru(II) and Rh(III) bis(terpyridine) complexes. *Inorg. Chem.* **2001**, *40*, 4986−4995.
(30) Yutaka, T.; Kurihara, M.; Kubo, K.; Nishihara, H. Novel photoisomerization behavior of Rh binuclear complexes involving azobenzene-bridged bis(terpyridine) ligand. Strong effects of counterion and solvent and the induction of redox potential shift. *Inorg. Chem.* **2000**, *39*, 3438−3439.
(31) Lin, L.-R.; Tang, H.-H.; Wang, Y.-G.; Wang, X.; Fang, X.-M.; Ma, L.-H. Functionalized lanthanide(III) complexes constructed from azobenzene derivative and β-diketone ligands: Luminescent, magnetic, and reversible trans-to-cis photoisomerization properties. *Inorg. Chem.* **2017**, *56*, 3889−3900.
(32) Souri, N.; Tian, P.; Platas-Iglesias, C.; Wong, K.-L.; Nonat, A.; Charbonniere, L. J. Upconverted photosensitization of Tb visible emission by NIR Yb excitation in discrete supramolecular heteropolynuclear complexes. *J. Am. Chem. Soc.* **2017**, *139*, 1456−1459.
(33) Doffek, C.; Seitz, M. The radiative lifetime in near-IR-luminescent ytterbium cryptates: The key to extremely high quantum yields. *Angew. Chem., Int. Ed.* **2015**, *54*, 9719−9721.
(34) Bischof, C.; Wahsner, J.; Scholten, J.; Trosien, S.; Seitz, M. Quantification of C-H Quenching in Near-IR Luminescent Ytterbium and Neodymium Cryptates. *J. Am. Chem. Soc.* **2010**, *132*, 14334−14335.
(35) Bunzli, J.-C. G. Lanthanide luminescence for biomedical analyses and imaging. *Chem. Rev.* **2010**, *110*, 2729−2755.
(36) Sun, L. N.; Dang, S.; Yu, J. B.; Feng, J.; Shi, L. Y.; Zhang, H. J. Near-Infrared Luminescence from visible-light-sensitized hybrid materials covalently linked with tris(8-hydroxyquinolinate)-lanthanide [Er(III), Nd(III), and Yb(III)] derivatives. *J. Phys. Chem. B* **2010**, *114*, 16393−16397.
(37) Boulon, G.; Collombet, A.; Brenier, A.; Cohen-Adad, M. T.; Yoshikawa, A.; Lebbou, K.; Lee, J. H.; Fukuda, T. Structural and spectroscopic characterization of nominal Yb^{3+}:$Ca_8La2(PO4)6O2$ oxyapatite single crystal fibers grown by the micro-pulling-down method. *Adv. Funct. Mater.* **2001**, *11*, 263.
(38) Ayers, K. M.; Schley, N. D.; Ung, G. Monometallic lanthanide salicylhydrazonecomplexes exhibiting strong near-infrared luminescence. *Chem. Commun.* **2019**, *55*, 8446−8449.
(39) Nonat, A.; Imbert, D.; Pecaut, J.; Giraud, M.; Mazzanti, M. Structural and photophysical studies of highly stable lanthanide complexes of tripodal 8-hydroxyquinolinate ligands based on 1,4,7-triazacyclononane. *Inorg. Chem.* **2009**, *48*, 4207−4218.
(40) Zhang, T.; Zhu, X.; Cheng, C. C. W.; Kwok, W.-M.; Tam, H.-L.; Hao, J.; Kwong, D. W. J.; Wong, W.-K.; Wong, K.-L. Water-soluble mitochondria-specific ytterbium complex with impressive NIR emission. *J. Am. Chem. Soc.* **2011**, *133*, 20120−20122.

https://dx.doi.org/10.1021/acs.inorgchem.0c02488
Inorg. Chem. XXXX, XXX, XXX−XXX